sustainability

MDPI

Article

Effect of Carboxylic Acids on Corrosion of Type 410 Stainless Steel in Pyrolysis Bio-Oil

Dino Sulejmanovic [1], James R. Keiser [1], Yi-Feng Su [1], Michael D. Kass [2], Jack R. Ferrell III [3], Mariefel V. Olarte [4], John E. Wade IV [1] and Jiheon Jun [1,*]

1 Material Science and Technology Division, Oak Ridge National Laboratory, Oak Ridge, TN 37830, USA
2 Buildings and Transportation Science Division, Oak Ridge National Laboratory, Oak Ridge, TN 37830, USA
3 National Renewable Energy Laboratory, Golden, CO 80401, USA
4 Pacific Northwest National Laboratory, Richland, WA 99354, USA
* Correspondence: junj@ornl.gov

Abstract: Biomass-derived oils are renewable fuel sources and commodity products and are proposed to partially or entirely replace fossil fuels in sectors generally considered difficult to decarbonize such as aviation and maritime propulsion. Bio-oils contain a range of organic compounds with varying functional groups which can lead to polarity-driven phase separation and corrosion of containment materials during processing and storage. Polar compounds, such as organic acids and other oxygenates, are abundant in bio-oils and are considered corrosive to structural alloys, particularly to those with a low-Cr content. To study the corrosion effects of small carboxylic acids present in pyrolysis bio-oils, type 410 stainless steel (SS410) specimens were exposed in bio-oils with varying formic, acetic, propionic and hexanoic acid contents at 50 °C during 48 h exposures. The specific mass change data show a linear increase in mass loss with increasing formic acid concentration. Interestingly, a mild corrosion inhibition effect on the corrosion of SS410 specimens was observed with the addition of acetic, propionic and hexanoic acids in the bio-oil.

Keywords: pyrolysis bio-oils; biomass; corrosion; carboxylic acid; stainless steel

check for updates

Citation: Sulejmanovic, D.; Keiser, J.R.; Su, Y.-F.; Kass, M.D.; Ferrell, J.R., III; Olarte, M.V.; Wade, J.E., IV; Jun, J. Effect of Carboxylic Acids on Corrosion of Type 410 Stainless Steel in Pyrolysis Bio-Oil. *Sustainability* **2022**, *14*, 11743. https://doi.org/10.3390/su141811743

Academic Editors: Akram Alfantazi, Ime Bassey Obot, Ambrish Singh and Ihsan ulhaq Toor

Received: 22 August 2022
Accepted: 12 September 2022
Published: 19 September 2022

Publisher's Note: MDPI stays neutral with regard to jurisdictional claims in published maps and institutional affiliations.

Copyright: © 2022 by the authors. Licensee MDPI, Basel, Switzerland. This article is an open access article distributed under the terms and conditions of the Creative Commons Attribution (CC BY) license (https://creativecommons.org/licenses/by/4.0/).

1. Introduction

Biomass-derived oils are considered as renewable sources of energy products or commodity chemicals [1–6]. They are produced by the thermochemical pyrolysis of biomass feedstocks from agricultural wastes, forest residues or other biomass sources [7–9]. Depending on the feedstock source and its processing conditions, these bio-oils can contain many organic compounds with various functional groups such as carboxyls, aldehydes, ketones, phenols and other oxygenates [10,11]. Some of these compounds can be corrosive to the structural alloys that are used during the processing and storage of bio-oils [12–17]. Over the years, our team has focused on understanding the compatibility of bio-oils with structural alloys, plastics and elastomers [18–23]. Several other groups studied the corrosion effects under the combustion conditions of biomass [24,25].

Ultimately, the presence of acidic oxygenates such as carboxylic acids is the main pathway leading to the degradation of structural materials in bio-oil environments. Due to their inability to form protective passivating oxide layers, alloys with low-Cr contents are particularly susceptible to corrosion attack in pyrolysis oils. Our previous studies showed that low-Cr alloys, after exposure in bio-oils, formed an iron formate dihydrate corrosion product on the surface of the alloy specimens [26]. These findings indicate a potential reaction pathway to the corrosion of alloys by the formic acid in bio-oils. Previously Sekine, Singh and coauthors studied the effects of varying formic acid concentration on the corrosion of low-Cr alloys and proposed a potential mechanism for formic acid attack on low-Cr alloys in aqueous conditions [27,28].

However, there are no reports showing the effects of carboxylic acid concentration on the corrosion of alloys in bio-oil environments. Herein, we exposed stainless steel type 410 (SS410) specimens (McMaster Carr, Inc., Elmhurst, IL, USA) in pyrolysis bio-oils and varied the amount of formic, acetic, propionic and hexanoic acids to study the concentration effects of acids on the corrosion of SS410.

2. Materials and Methods

2.1. Corrosion Exposure

Type 410 stainless steel (SS410) coupons (2~2.5 mm thickness) with the chemical composition shown in Table 1 were cut from a rod with approximately 16 mm diameter. A~1 mm hole was drilled in each coupon. The SS410 coupons were then polished to 600-grit finish, cleaned with acetone and ethanol and were weighed to ±0.04 mg accuracy using a Mettler Toledo XP205 balance (Mettler-Toledo, Columbus, OH, USA). Then the coupons were hung with a Teflon wire as shown in Figure 1. Approximately 25–27 g of high-ash and high-moisture bio-oil, referred to as FR3 bio-oil from now on, produced by the National Renewable Energy Laboratory (Golden, CO, USA) [29] was weighed and placed into 40 mL glass vials. Further characterization of this FR3 bio-oil is described elsewhere [29,30].

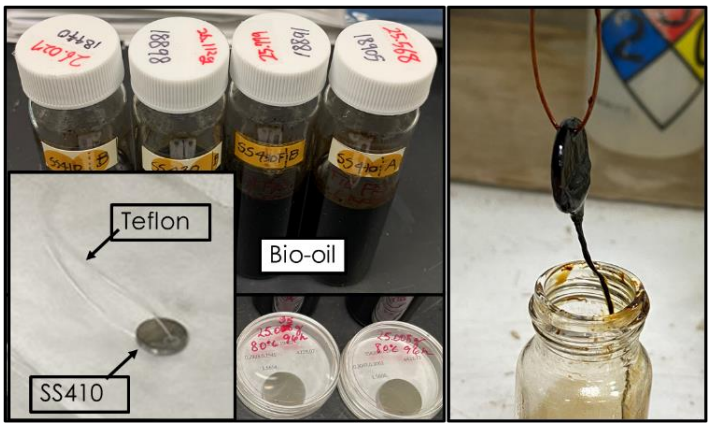

Figure 1. Photos showing bio-oils contained in glass vials (~100 mm tall, **top left**), SS410 coupon with Teflon wire (**bottom left**), two as-prepared SS410 coupons (**bottom middle**) and a SS410 coupon retrieved from bio-oil after exposure (**right**). The diameter of SS410 coupons is ~16 mm.

One end of a Teflon wire (the other end with a coupon) was attached to a plastic vial cap by making a hole in the inner liner of the vial cap. Bio-oil corrosion exposures were initiated by placing the SS410 coupons into the bio-oil liquid. The vial cap was closed, and the vial was placed inside a temperature-controlled oven at 50 °C for 48 h. The corrosion exposure tests were triplicated for statistic confidence. After 48 h exposure, coupons were removed from the oil and placed in a vial containing 10 mL of methanol for 5 min. The coupons were then removed from methanol and were rinsed with acetone to clean off any remaining oil. To avoid potential methoxylation of SS410 surface during the cleaning [31], the immersion time in methanol did not exceed 5 min. After this initial cleaning, the samples were further cleaned using a mineral oil-based rust remover solution in an ultrasonic bath. Coupons were weighed, and mass change data were obtained.

Table 1. Elemental composition of SS410 coupons determined by inductively coupled plasma technique [32–34].

Alloy	Cr	Mn	Fe	Ni	Cu	Si	C	N	O	S
SS410	11.9	0.47	Balance	0.23	0.16	0.3	0.13	0.012	0.0026	<0.001

2.2. ICP-MS Elemental Analysis

Bio-oils were digested using a mixed acid method with the aid of microwave Teflon bomb digestion. Then, 0.25 mL of sample was mixed with 1.5 mL of 16 M nitric acid and was left overnight. To the bio-oil and nitric acid mixture, 0.5 mL of 12 M hydrochloric and 0.2 mL of hydrofluoric acid were added. The mixture was placed in a high-pressure microwave rotor (SK15) and heated to 205 °C. After microwave digestion, the mixture was diluted to 15 mL volume, and another 1:5 dilution was prepared for the ICP-MS analysis. The measurements were performed using a magnetic sector ICP-MS (Thermo-Finnigan Element XR) instrument (Thermo Fisher Scientific, Waltham, MA, USA).

2.3. Capillary Electrophoresis (CE)

Carboxylate anions were quantified using the capillary electrophoresis method. Bio-oil samples were prepared using a liquid–liquid extraction. Approximately 0.5 g of bio-oil was weighed and mixed with 5 mL of deionized water. The mixture was sonicated for one hour according to the previously published procedure [35]. The aqueous extract was diluted and used in an Agilent 7100 (Agilent Technologies, Santa Clara, CA, USA) CE instrument with a 72 cm, 75 µm ID capillary with indirect UV detection at 350 nm and reference at 200 nm using −30 kV.

3. Results

Figure 2 shows the specific mass change data of SS410 coupons exposed in FR3 bio-oil with varying amounts of formic acid additions. Two different methods of formic acid additions were used. First, a 10 wt.% solution of formic acid was prepared from a 90 wt.% formic acid. The 10 wt.% formic acid solution was measured with an Eppendorf E3 Repeater pipette and was added to the ~25 g of bio-oil liquid. The liquid was vigorously mixed with a vortex before using the oil + acid mixture for SS410 corrosion exposure. The black circle data points in Figure 2 are from the 10 wt.% formic acid additions to the FR3 bio-oil.

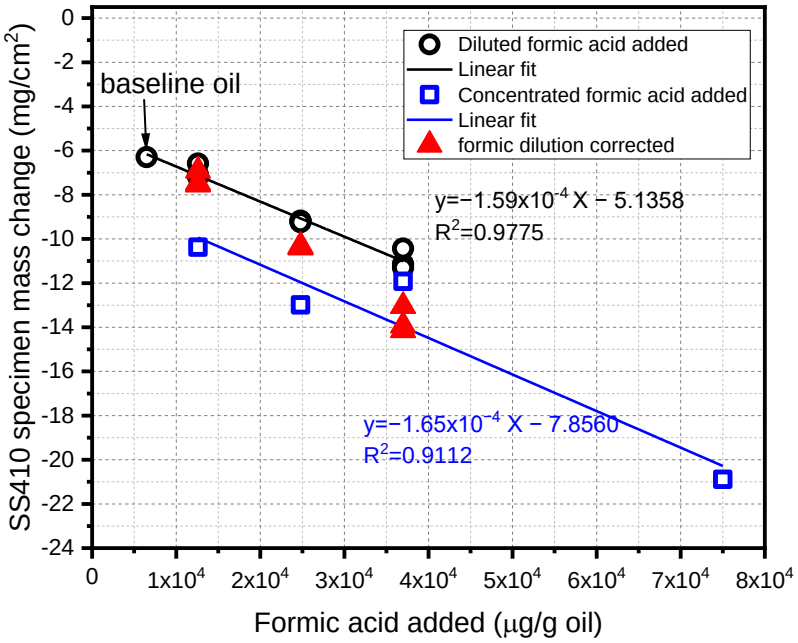

Figure 2. SS410 specimen mass change vs. added formic acid in FR3 bio-oil for exposure at 50 °C for 48 h. Two different methods of adding formic acid were used, one with 10 wt.% formic acid solution and another with concentrated formic acid. Dilution correction to the diluted formic acid data (black circles) was performed by normalizing to the same volume as with concentrated data points (blue squares).

The second method for formic acid additions to the bio-oil was using a concentrated formic acid (90 wt.%). The acid was measured with an Eppendorf E3 Repeater and was added to the bio-oil. The mixture of the bio-oil and concentrated acid was vigorously shaken using a vortex machine. SS410 coupons were then exposed in the mixtures of bio-oil and formic acid for 48 h at 50 °C. The data for the concentrated formic acid additions to the bio-oil are shown in Figure 2 in the blue square data points. The red triangles are showing the dilution correction performed on the diluted addition data points (black circles). The black and blue lines are linear fits for the 10 wt.% and concentrated formic acid additions, respectively. Linear equations and R^2 values are also shown in respective colors.

The mass change data plot of SS410 coupons vs. added acetic acid content is shown in Figure 3. Acetic acid additions were performed using two methods. The first method was by adding a diluted acetic acid solution (10 wt.%), and the second was by adding a glacial acetic acid (99.7 wt.%). The black circles are the mass change data obtained from the 10 wt.% acetic acid additions. The blue square data points are data obtained from the concentrated acetic acid additions. The red triangles are the dilution-corrected data points. The lines represent crude fits to the data points and are only for a visual guide. The decreasing mass loss with increasing acetic acid concentration (black points) suggests a mild inhibitory effect on the corrosion of SS410 coupons when diluted acetic acid was added.

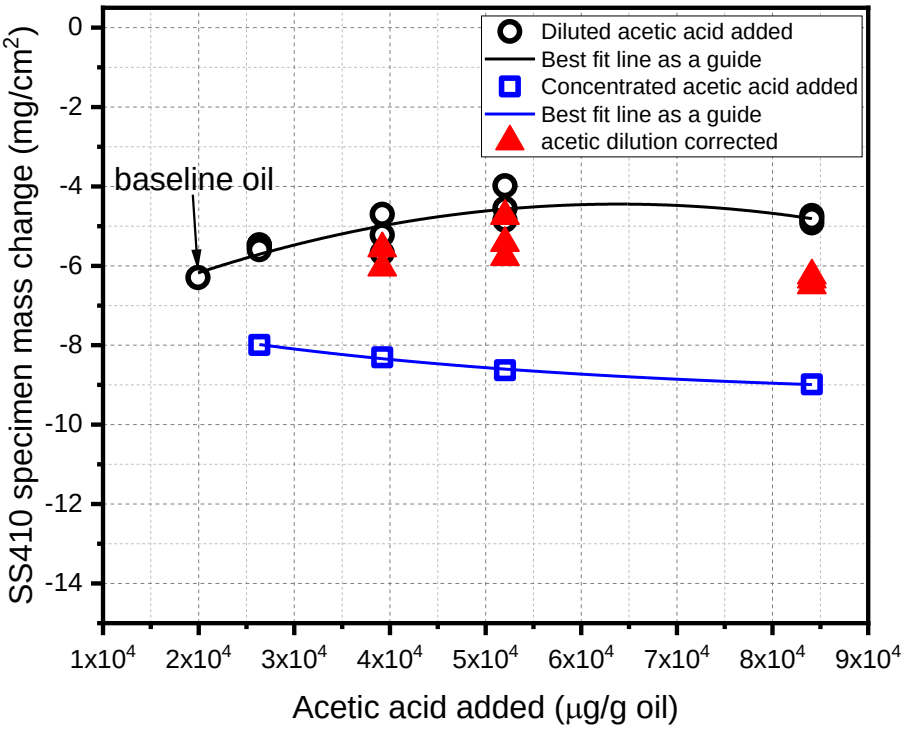

Figure 3. SS410 specimen mass change vs. added acetic acid in FR3 bio-oil for exposure at 50 °C for 48 h. Two different methods of adding formic acid were used, one with 10 wt.% acetic acid solution and another with concentrated acetic acid. Dilution correction to the diluted acetic acid data (black circles) was performed by normalizing to the same volume as with concentrated data points (blue squares).

Figure 4 shows the results of the capillary electrophoresis analysis of FR3 bio-oil. The electrophoretogram of the standard solution sample that contained 12 different carboxylate anions is shown in Figure 4a. Figure 4b shows the electrophoretogram of the FR3 bio-oil sample with five different carboxylate anions detected using capillary electrophoresis. The peaks labeled 1 and 2 are formate and acetate anions, respectively. The area under the curve for each peak was obtained and used to determine the concentrations of carboxylate anions in the bio-oil mixture samples.

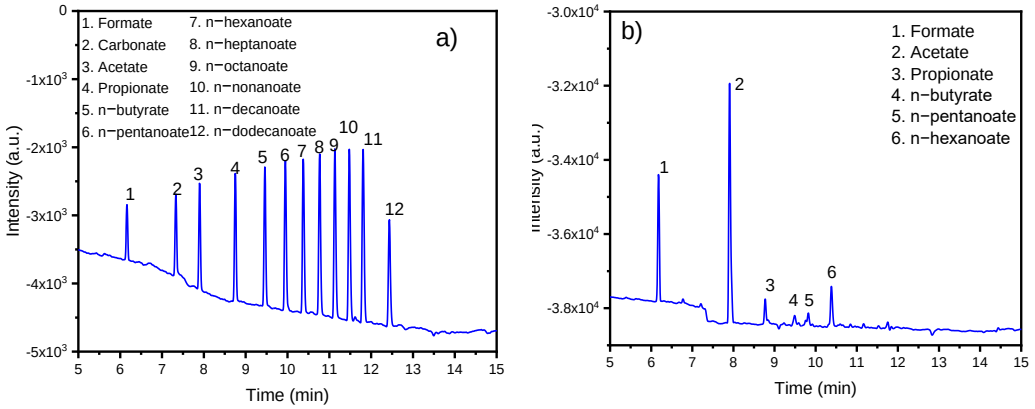

Figure 4. Capillary electrophoretograms for (**a**) standard solution showing straight-chain carboxylate anions and (**b**) an extract sample of FR3 bio-oil sample showing the detection of straight-chain carboxylate anion.

The SEM microscopy and elemental maps of the SS410 specimen cross-section after exposure in FR3 bio-oil is shown in Figure 5. Cr, Fe, Mn and Si maps were obtained to determine the compositional variations of each element in the substrate and at the surface where the alloy interfaces with the bio-oil. As the corrosive species in bio-oils contain oxygen, elemental maps of oxygen were obtained to determine if corrosion products formed on the surface of the SS410 specimens.

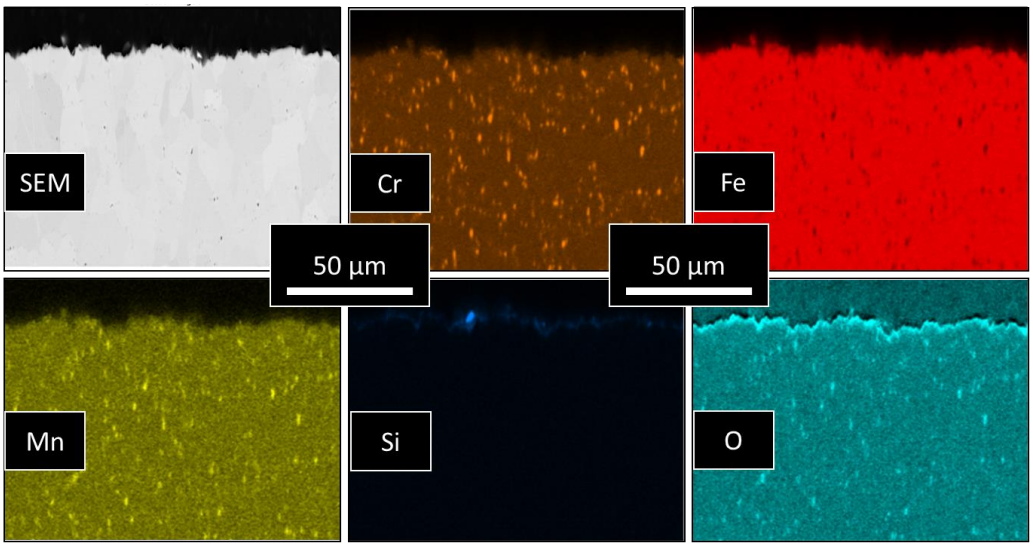

Figure 5. SEM and elemental maps of the cross-section of SS410 specimen after exposure in FR3 bio-oil at 50 °C for 48 h.

To show the homogenous surface corrosion attack on the bio-oil-exposed specimens, surface plane view SEM and elemental maps were collected using SEM-EDS as presented in Figure 6. Cr and Fe, as major elements in SS410, were mapped to determine any possible variations in composition at the surface of the specimens. Overall, uniform distribution of Fe and Cr, except Cr-enriched spots, was observed in the roughened SS410 surfaces (Figure 6a). The exposed surfaces showed etched morphologies in both formic and acetic acid cases, but the contrast of such morphology was more apparent when formic acid was added to the bio-oil (Figure 6b).

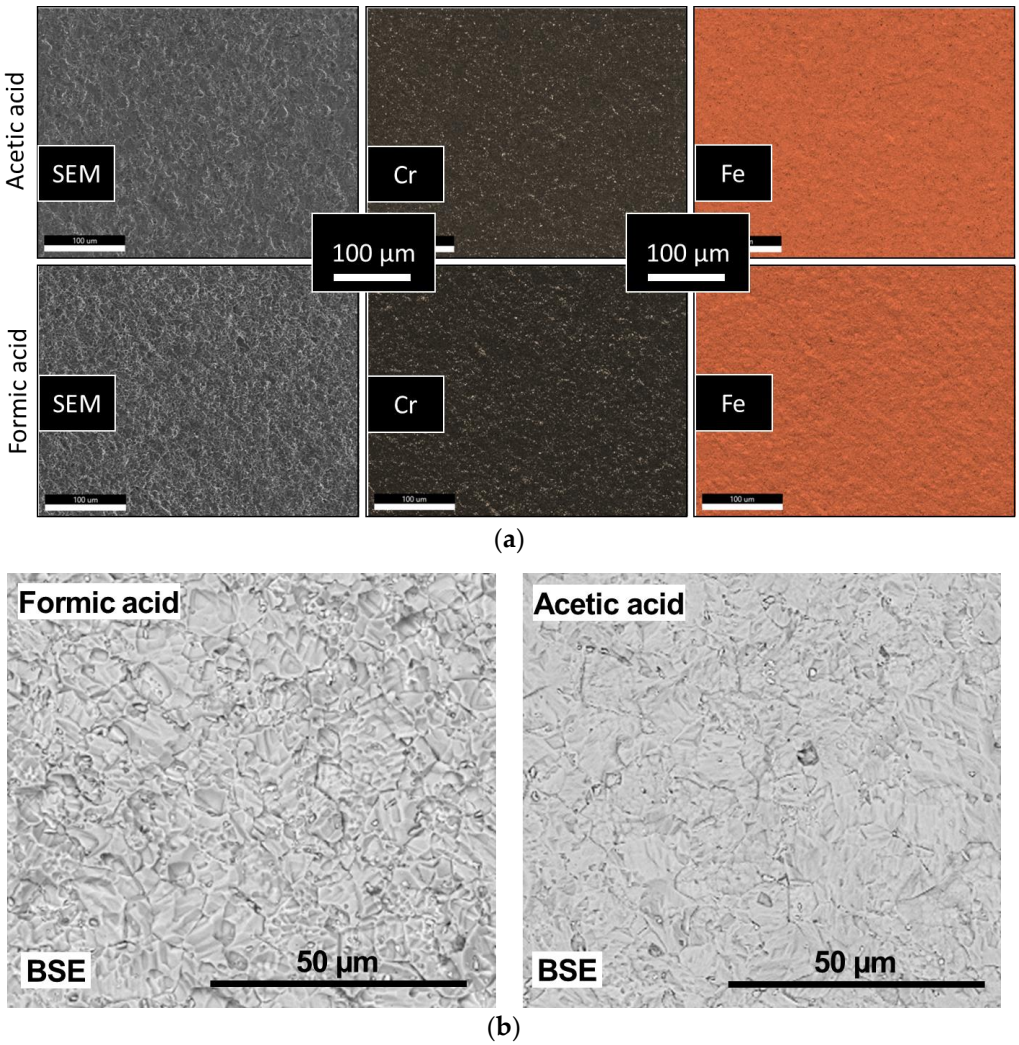

Figure 6. Plane view comparison of postexposure SS410 surfaces in bio-oils added with equivalent mol amounts (800 µmol) of acetic or formic acid. (**a**) Secondary electron SEM images and their EDS elemental maps and (**b**) BSE (back-scattered electron) images from other locations in a higher magnification.

To study the effect of the carboxylic acid type/size and their corrosivity towards SS410, we exposed alloy specimens in bio-oils containing additions of propionic and hexanoic acids. The specific mass change plot of SS410 specimens exposed in FR3 bio-oil after additions of propionic acid is shown in Figure 7. The black circles are data obtained from individual specimens, and the blue line is the linear fit of the data with the linear equation presented along with the R^2 value. The specific mass change plot of SS410 specimens exposed in FR3 bio-oil after additions of hexanoic acid is shown in Figure 8. The black circles are data obtained from individual specimens, and the blue line is the linear fit of the data with the linear equation shown along with the R^2 value.

Table 2 shows the ICP-MS analysis of the baseline bio-oil after SS410 exposures for 48 h at 50 °C. The major alloying elements present in SS410 (Cr, Mn and Fe) were analyzed, and the results are summarized below. Comparison of the total elemental composition (Cr + Mn + Fe) determined using ICP-MS with the measured mass loss of the SS410 specimens is also shown in Table 2.

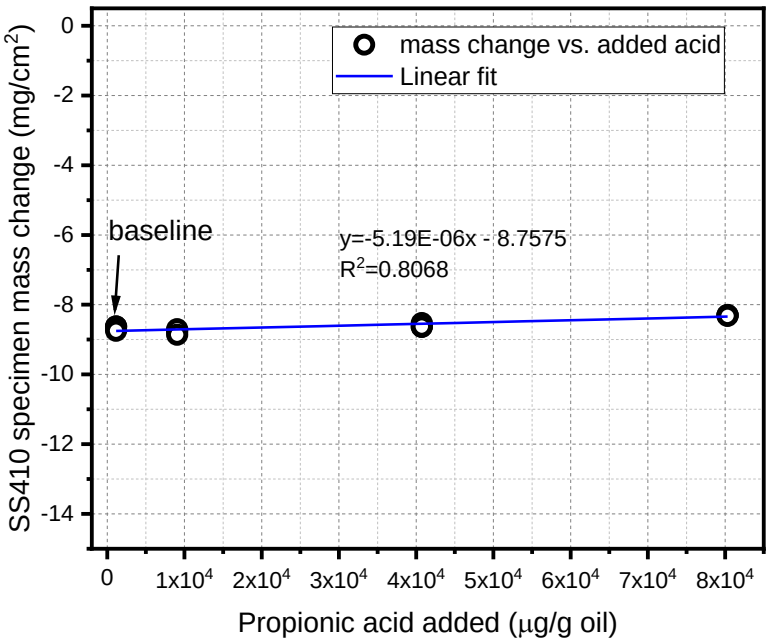

Figure 7. SS410 specimen specific mass change vs. added propionic acid in FR3 bio-oil for exposure at 50 °C for 48 h.

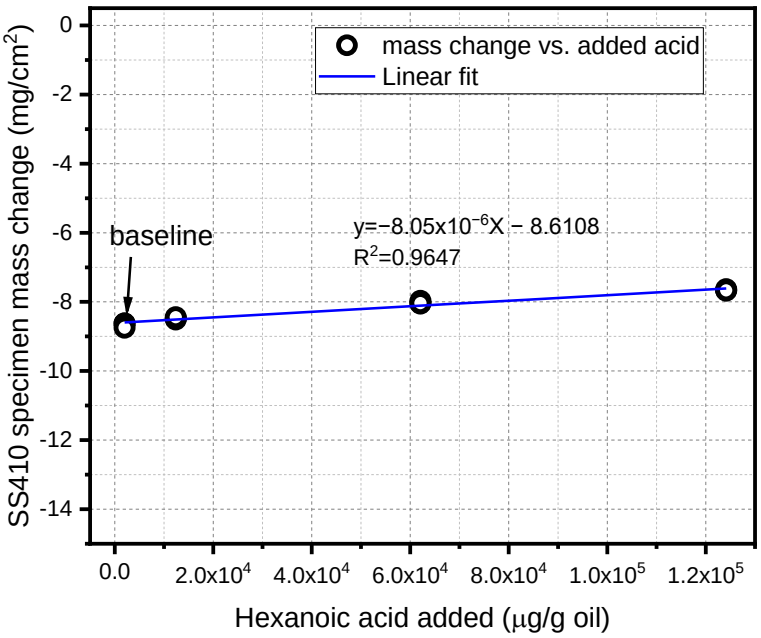

Figure 8. SS410 specific specimen mass change vs. added hexanoic acid in FR3 bio-oil for exposure at 50 °C for 48 h.

Table 2. ICP-MS of bio-oil after SS410 exposures in the baseline FR3 oil. Values in parentheses are standard deviations.

Run # for FR3 Bio-Oil	ICP-MS, μg/g Oil			ICP Total (Cr + Mn + Fe) (mg)	Measured Mass Loss (mg)	Deviation (%)
	Cr	Mn	Fe			
1	91.2 (32.9)	4.55 (1.4)	795 (105)	23.18	29.70	21.94
2	94.1 (33.9)	4.62 (1.4)	771 (101)	22.24	27.92	20.35
3	92.7 (33.4)	4.55 (1.4)	849 (113)	24.43	28.80	15.19
4	96.3 (34.7)	4.88 (1.5)	867 (116)	24.54	29.08	15.62

4. Discussion

Fast pyrolysis bio-oils contain a range of organic compounds with varying functional groups. Oxygen-containing organic compounds can potentially be corrosive to alloys due to the oxyphilic nature of the alloying elements. One of the main concerns for alloy corrosion in bio-oils is the presence of organic acids. Carboxylic acids can be particularly corrosive to low-chromium steels and carbon steels due to the inability of these alloys to form a passivating oxide layer characteristic of higher Cr alloys [28,36]. To study the effect of carboxylic acids on alloy corrosion, we exposed SS410 coupons in a pyrolysis bio-oil (FR3) with and without deliberate additions of formic, acetic, propionic and hexanoic acids using the method we recently developed and as illustrated in Figure 1 [37].

The initial characterization of FR3 fast pyrolysis oil was performed using the aqueous modified total acid number (AMTAN) to determine the acidity of the oil and using capillary electrophoresis to quantify the carboxylate anions present in the bio-oil. The AMTAN is a value of total acid present in a bio-oil measured using acid-base titration of the aqueous extract using a standardized KOH solution. Two samples of FR3 oil were subjected to KOH titrations and yielded 50.26 and 49.93 mg of KOH per gram of bio-oil. These values are significantly lower compared to some of the previously measured AMTAN values in fast pyrolysis bio-oils [30,38,39]. The observed lower AMTAN values are potentially due to the aging of the pyrolysis oils over time as described by Black and Ferrell [40].

Our previous results of long-term alloy exposures in pyrolysis bio-oils showed that alloy SS410 is susceptible to corrosion in pyrolysis oil liquids and the vapor phase [38]. As concluded from our previous studies, the general trend of alloy degradation in bio-oil environments is correlated to the composition of chromium in the alloy. Alloys with higher Cr concentration generally perform better than ones with lower Cr content in pyrolysis bio-oils [17]. The major corrosion product that was consistently detected on the surface of the low-Cr alloys after exposures in pyrolysis bio-oils was iron formate dihydrate which likely formed through the reaction of Fe in the alloy surface and the formic acid present in bio-oils [27].

When looking at the carboxylic acid concentrations in bio-oils, formic and acetic acids are the major carboxylic acids present as described in previous reports [38] and as shown by the capillary electrophoresis results in Figure 4. Carboxylate anion peaks shown in Figure 4 were well resolved in under 13 min. While previously reported results suggest the link between carboxylic acids and alloy corrosion in bio-oils, we found no reports that attempted to correlate the extent of alloy degradation by varying the concentration of carboxylic acids in bio-oils. Herein, we exposed SS410 specimens in bio-oil with varying concentrations of formic, acetic, propionic and hexanoic acids. As several conditions and specimens needed to be studied in these experiments, short-term (48 h) SS410 bio-oil exposures at 50 °C were chosen in order to provide relatively quick results about the degradation of SS410 in pyrolysis bio-oils [30].

The specific mass change plot of SS410 specimens after exposure in FR3 pyrolysis oil shows increasing mass loss as a function of added formic acid (Figure 2). The SS410 specimens exposed in the baseline FR3 bio-oil showed an average mass loss of 6.1 mg/cm^2 which equates to about a 1.48 mm/yr corrosion rate. The corrosion rates varied from 1.48 mm/yr for the baseline oil to 4.93 mm/yr for the highest addition of formic acid. The baseline bio-oil corrosion rate is comparable to that of SS410 exposed in 1 M HCl at room temperature [41] and 20% NaCl aqueous solutions at 80 °C [42]. Increasing the concentration of formic acid in the bio-oil resulted in a linear trend of mass loss which suggests that formic acid plays a major role in low-Cr steel corrosion in bio-oil environments. The method by which the formic acid was introduced into the bio-oil did not affect the general trend of mass loss as a function of the acid added. However, a small offset in the data between 10 wt.% vs. concentrated formic acid additions, as indicated by the y-intercepts of the two lines, suggests that the addition of water along with the acid made the bio-oil slightly less corrosive which could be due to the dilution effect and improved diffusion when 10 wt.% formic acid solution was used to add formic acid.

Unlike the formic acid results, when 10 wt.% acetic acid was added to the bio-oil, the specific mass loss of SS410 specimens slightly decreased compared to the concentrated acid results, as shown in Figure 3. The decrease in mass loss of SS410 specimens compared to those exposed in the baseline oil suggests the inhibition effect of diluted acetic acid on the corrosion of SS410 in pyrolysis bio-oil. When concentrated acetic acid was added to the bio-oil, the mass change data showed slight mass loss in the exposed SS410 specimens. Dilution-corrected mass change values are shown in Figures 2 and 3 (red triangles) and indicate that the dilution of formic and acetic acids affected the mass change data at higher acid concentrations. However, at lower concentrations, the correction did not significantly affect the data which may indicate other factors such as nonlinear specific mass change response to dilutions or acid diffusion limitations at lower concentrations.

To analyze the extent of the corrosive attack on SS410 specimens, characterization of the postexposure samples in cross-section and surface plane views were performed using scanning electron microscopy coupled with energy dispersive X-ray spectroscopy (SEM-EDS). EDS elemental maps show the equal distribution of alloying elements, Cr, Mn, and Fe, close to the surface and within the bulk of the specimens which suggests a nonpreferential corrosion attack by congruent metal dissolution. A small layer of oxide was detected on the surface which could be due to the formation of iron formate dihydrate as previously observed in bio-oils. The plane view SEM images and Cr and Fe elemental maps of postexposure SS410 surfaces, presented in Figure 6a,b, show etched morphologies indicating a relatively homogenous attack, without any corrosion ditch or deep pit, in the observed area.

The specific mass change plots for propionic and hexanoic acids, plotted in Figures 7 and 8, show very little change as a function of added acid. In both cases, the mass loss slightly decreased with increasing the acid added which suggests a minor inhibition effects of propionic and hexanoic acids on the corrosion of SS410. It is worthwhile noting that both propionic and hexanoic acids were added undiluted to the bio-oil.

5. Conclusions

SS410 alloy specimens were exposed in pyrolysis bio-oil with varying amounts of four carboxylic acids. The corrosion of SS410 alloy was assessed using mass change data, surface and cross-sectional electron microscopy images and elemental mapping of the exposed specimens. The carboxylic acids were separated and quantified using capillary electrophoresis. Corrosion exposures revealed a linear correlation of SS410 mass loss with the amount of formic acid added to the bio-oil, indicating that formic acid is the most aggressive among the four acids tested. Interestingly, the addition of acetic, propionic and hexanoic acids showed a mild inhibitory effect on the corrosion of SS410 specimens.

Author Contributions: Conceptualization, D.S., J.J. and J.R.K.; Methodology, D.S., J.J. and J.R.K.; Validation, D.S., J.J., J.R.F.III, M.V.O. and M.D.K.; Experiments, D.S., J.E.W.IV; Characterization, Y.-F.S. All authors have read and agreed to the published version of the manuscript.

Funding: This research was funded by DOE Bioenergy Technologies Office, DE-AC05-00OR22725.

Informed Consent Statement: Not applicable.

Acknowledgments: This research was funded by the Bioenergy Technologies Office of the U.S. Department of Energy. Timothy Theiss, Sebastien Dryepondt, Mackenzie Ridley and Mathew Kurley at ORNL provided useful comments for this manuscript. This manuscript has been authored by UT-Battelle, LLC under Contract No. DE-AC05-00OR22725 with the U.S. Department of Energy. The United States Government and the publisher, by accepting the article for publication, acknowledges that the United States Government retains a nonexclusive, paid-up, irrevocable, worldwide license to publish or reproduce the published form of this manuscript or allow others to do so, for United States Government purposes. The Department of Energy will provide public access to these results of federally sponsored research in accordance with the DOE Public Access Plan (http://energy.gov/downloads/doe-public-access-plan (accessed on 11 September 2022)).

Conflicts of Interest: The authors declare no conflict of interest.

References

1. Czernik, S.; Bridgwater, A.V. Overview of Applications of Biomass Fast Pyrolysis Oil. *Energy Fuels* **2004**, *18*, 590–598. [CrossRef]
2. Huber, G.W.; Iborra, S.; Corma, A. Synthesis of Transportation Fuels from Biomass: Chemistry, Catalysts, and Engineering. *Chem. Rev.* **2006**, *106*, 4044–4098. [CrossRef] [PubMed]
3. Downing, M.; Eaton, L.M.; Graham, R.L.; Langholtz, M.H.; Perlack, R.D.; Turhollow, J.A.F.; Stokes, B.; Brandt, C.C. *U.S. Billion-Ton Update: Biomass Supply for a Bioenergy and Bioproducts Industry*; U.S. Department of Energy: Washington, DC, USA, 2011.
4. Zhang, X.-S.; Yang, G.-X.; Jiang, H.; Liu, W.-J.; Ding, H.-S. Mass production of chemicals from biomass-derived oil by directly atmospheric distillation coupled with co-pyrolysis. *Sci. Rep.* **2013**, *3*, 1120. [CrossRef]
5. Zacher, A.H.; Olarte, M.V.; Santosa, D.M.; Elliott, D.C.; Jones, S.B. A review and perspective of recent bio-oil hydrotreating research. *Green Chem.* **2014**, *16*, 491–515. [CrossRef]
6. Elkasabi, Y.; Mullen, C.A.; Boateng, A.A. Distillation and Isolation of Commodity Chemicals from Bio-Oil Made by Tail-Gas Reactive Pyrolysis. *ACS Sustain. Chem. Eng.* **2014**, *2*, 2042–2052. [CrossRef]
7. Butler, E.; Devlin, G.; Meier, D.; McDonnell, K. A review of recent laboratory research and commercial developments in fast pyrolysis and upgrading. *Renew. Sustain. Energy Rev.* **2011**, *15*, 4171–4186. [CrossRef]
8. Bridgwater, A.V. Upgrading biomass fast pyrolysis liquids. *Environ. Prog. Sustain. Energy* **2012**, *31*, 261–268. [CrossRef]
9. Carpenter, D.; Westover, T.L.; Czernik, S.; Jablonski, W. Biomass feedstocks for renewable fuel production: A review of the impacts of feedstock and pretreatment on the yield and product distribution of fast pyrolysis bio-oils and vapors. *Green Chem.* **2014**, *16*, 384–406. [CrossRef]
10. Christensen, E.D.; Chupka, G.M.; Luecke, J.; Smurthwaite, T.; Alleman, T.L.; Iisa, K.; Franz, J.A.; Elliott, D.C.; McCormick, R.L. Analysis of Oxygenated Compounds in Hydrotreated Biomass Fast Pyrolysis Oil Distillate Fractions. *Energy Fuels* **2011**, *25*, 5462–5471. [CrossRef]
11. Lyu, G.; Wu, S.; Zhang, H. Estimation and Comparison of Bio-Oil Components from Different Pyrolysis Conditions. *Front. Energy Res.* **2015**, *3*, 28. [CrossRef]
12. Czernik, S. Storage of biomass pyrolysis oils. In Proceedings of the Storage of Biomass Pyrolysis Oils—Proceedings of Biomass Pyrolysis Oil Properties and Combustion Meeting, Estes Park, CO, USA, 26–28 September 1994; NREL CP-4397215. pp. 26–28.
13. Oasmaa, A.; Czernik, S. Fuel Oil Quality of Biomass Pyrolysis OilsState of the Art for the End Users. *Energy Fuels* **1999**, *13*, 914–921. [CrossRef]
14. Ropital, F. Current and future corrosion challenges for a reliable and sustainable development of the chemical, refinery, and petrochemical industries. *Mater. Corros.* **2009**, *60*, 495–500. [CrossRef]
15. Keiser, J.R.; Brady, M.P.; Lewis, S.S.A.; Connatser, R.M.; Leonard, D.N.; Whitmer, L. Impact of corrosion on selection of structural materials for thermochemical processing of biomass. In Proceedings of the TAPPI PEERS 2014, Tacoma, WA, USA, 15 September 2014.
16. Keiser, J.R.; Brady, M.P.; Thomson, J.K.; Connatser, R.M.; Lewis, S.A., Sr.; Leonard, D.N. BBio-Oil Properties and Effects on Containment Materials. In Proceedings of the NACE CORROSION Conference, San Antonio, TX, USA, 9–13 March 2014. NACE-2014-4423.
17. Jun, J.; Sulejmanovic, D.; Keiser, J.; Brady, M.; Kass, M. Evaluation of Corrosion Susceptibility of Structural Steels in Biomass Derived Pyrolysis Oil. In Proceedings of the NACE CORROSION Conference 2021, Virtual, 19 April 2021. Paper No. 16502.
18. Keiser, J.; Brady, M.P.; Connatser, R.; Lewis, S. Degradation of structural alloys in biomass-derived pyrolysis oil. *J. Sci. Technol. For. Prod. Processes* **2013**, *3*, 16–22.
19. Kass, M.D.; Janke, C.J.; Connatser, R.M.; Lewis, S.A.; Keiser, J.R.; Gaston, K. Compatibility Assessment of Fuel System Elastomers with Bio-oil and Diesel Fuel. *Energy Fuels* **2016**, *30*, 6486–6494. [CrossRef]
20. Kass, M.D.; Janke, C.J.; Connatser, R.M.; Lewis, S.A.; Keiser, J.R.; Gaston, K. Compatibility Assessment of Fuel System Infrastructure Plastics with Bio-oil and Diesel Fuel. *Energy Fuels* **2018**, *32*, 542–553. [CrossRef]
21. Jun, J.; Sulejmanovic, D.; Keiser, J.; Brady, M.; Kass, M. Corrosion Behavior of Alloy Structural Steels in Catechol and Biomass-Derived Pyrolysis Oils. In Proceedings of the NACE CORROSION Conference 2021, Virtual, 19 April 2021. Paper No. 16361.
22. Jun, J.; Sulejmanovic, D.; Keiser, J.R.; Brady, M.P.; Kass, M.D. Electrochemical Corrosion Analysis of Stainless Steels in LALM Pyrolysis Bio-Oil with Organic Corrodents. In Proceedings of the AMPP CORROSION Conference 2022, San Antonio, TX, USA, 6–10 March 2022. Paper No.17759.
23. Kass, M.D.; Janke, C.J.; Lobodin, V.V.; Bras, W.; Keiser, J.R.; Sulejmanovic, D.; Jun, J. Compatibility of Fuel System Elastomers and Plastics with a Fast-Pyrolysis Oil (Bio-oil) at Room Temperature. *Energy Fuels* **2022**, *36*, 9158–9170. [CrossRef]
24. Antunes, R.A.; de Oliveira, M.C.L. Corrosion in biomass combustion: A materials selection analysis and its interaction with corrosion mechanisms and mitigation strategies. *Corros. Sci.* **2013**, *76*, 6–26. [CrossRef]
25. Okoro, S.C.; Montgomery, M.; Frandsen, F.J.; Pantleon, K. High Temperature Corrosion under Laboratory Conditions Simulating Biomass-Firing: A Comprehensive Characterization of Corrosion Products. *Energy Fuels* **2014**, *28*, 6447–6458. [CrossRef]
26. Keiser, J.R.; Howell, M.; Lewis Sr, S.; Connatser, R.M. Corrosion Studies Of Raw and Treated Biomass-Derived Pyrolysis Oils. In Proceedings of the NACE CORROSION Conference 2012, Salt Lake City, UT, USA, 11–15 March 2012. C2012-0001645.
27. Sekine, I.; Ohkawa, H.; Handa, T. The corrosion behaviour and hydrogen evolution reaction of Fe in non-aqueous formic acid. *Corros. Sci.* **1982**, *22*, 1113–1123. [CrossRef]
28. Singh, M.M.; Gupta, A. Corrosion behaviour of mild steel in formic acid solutions. *Mater. Chem. Phys.* **1996**, *46*, 15–22. [CrossRef]

29. Klinger, J.; Carpenter, D.L.; Thompson, V.S.; Yancey, N.; Emerson, R.M.; Gaston, K.R.; Smith, K.; Thorson, M.; Wang, H.; Santosa, D.M.; et al. Pilot Plant Reliability Metrics for Grinding and Fast Pyrolysis of Woody Residues. *ACS Sustain. Chem. Eng.* **2020**, *8*, 2793–2805. [CrossRef]
30. Jun, J.; Warrington, G.L.; Keiser, J.R.; Connatser, R.M.; Sulejmanovic, D.; Brady, M.P.; Kass, M.D. Corrosion of Ferrous Structural Alloys in Biomass Derived Fuels and Organic Acids. *Energy Fuels* **2021**, *35*, 12175–12186. [CrossRef]
31. Lelek-Borkowska, U.; Palumbo, G.; Banaś, J. The Effect of the Methanol–Water Interaction on the Surface Layer on Titanium in CH_3OH-H_2O-$LiClO_4$ Solutions. *Electrochem* **2020**, *1*, 87–103. [CrossRef]
32. Connatser, R.M.; Frith, M.G.; Jun, J.; Lewis Sr, S.A.; Brady, M.P.; Keiser, J.R. Approaches to Investigate the Role of Chelation in the Corrosivity of Biomass-Derived Oils. *Biomass Bioenergy* **2020**, *133*, 105446. [CrossRef]
33. Jun, J.; Frith, M.G.; Connatser, R.M.; Keiser, J.R.; Brady, M.P.; Lewis, S. Corrosion Susceptibility of Cr–Mo Steels and Ferritic Stainless Steels in Biomass-Derived Pyrolysis Oil Constituents. *Energy Fuels* **2020**, *34*, 6220–6228. [CrossRef]
34. Jun, J.; Frith, M.G.; Connatser, R.M.; Keiser, J.R.; Brady, M.P.; Lewis, S., Sr. Corrosion of Ferrous Alloys by Organic Compounds in Simulated Bio-Oils. In Proceedings of the CORROSION 2019, Nashville, TN, USA, 24–28 March 2019. NACE-2019-12895, Paper No. 12895.
35. Connatser, R.M.; Lewis, S.A.; Keiser, J.R.; Choi, J.-S. Measuring bio-oil upgrade intermediates and corrosive species with polarity-matched analytical approaches. *Biomass Bioenergy* **2014**, *70*, 557–563. [CrossRef]
36. Jun, J.; Holguin, K.; Frankel, G.S. Pitting Corrosion of Very Clean Type 304 Stainless Steel. *Corrosion* **2013**, *70*, 146–155. [CrossRef]
37. Sulejmanovic, D.; Jun, J.; Keiser, J.R.; Connatser, R.M.; Lewis, S.A.; Christensen, E.D.; Ferrell Iii, J.R. *Corrosivity Screening of Pyrolysis Bio-Oils by Short-Term Alloy Exposures*; Laboratory Analytical Procedure (LAP); NREL: Golden, CO, USA, 2022.
38. Keiser, J.R.; Warrington, G.L.; Lewis, S.A., Sr.; Connatser, R.M.; Jun, J.; Qu, J.; Lee, K.; Brady, M.P. Corrosion and Chemical Characterization of Bio-Oils from Biomass with Varying Ash and Moisture Contents. In Proceedings of the NACE CORROSION Conference 2021, Virtual, 19 April 2021. Paper No. 16726.
39. Kass, M.D.; Armstrong, B.L.; Kaul, B.C.; Connatser, R.M.; Lewis, S.; Keiser, J.R.; Jun, J.; Warrington, G.; Sulejmanovic, D. Stability, Combustion, and Compatibility of High-Viscosity Heavy Fuel Oil Blends with a Fast Pyrolysis Bio-Oil. *Energy Fuels* **2020**, *34*, 8403–8413. [CrossRef]
40. Black, S.; Ferrell, J.R. Accelerated aging of fast pyrolysis bio-oil: A new method based on carbonyl titration. *RSC Adv.* **2020**, *10*, 10046–10054. [CrossRef]
41. Loto, R.T. Study of the corrosion behaviour of S32101 duplex and 410 martensitic stainless steel for application in oil refinery distillation systems. *J. Mater. Res. Technol.* **2017**, *6*, 203–212. [CrossRef]
42. Prifiharni, S.; Sugandi, M.T.; Pasaribu, R.R.; Sunardi, S.; Mabruri, E. Investigation of corrosion rate on the modified 410 martensitic stainless steel in tempered condition. *IOP Conf. Ser. Mater. Sci. Eng.* **2019**, *541*, 012001. [CrossRef]